JGR Biogeosciences

RESEARCH ARTICLE
10.1029/2021JG006505

Seasonal Hydroclimate Recorded in High Resolution $\delta^{18}O$ Profiles Across *Pinus palustris* Growth Rings

William E. Lukens[1], Robert T. Narmour[2], and Brian A. Schubert[2]

[1]Department of Geology and Environmental Science, James Madison University, Harrisonburg, VA, USA, [2]School of Geosciences, University of Louisiana at Lafayette, Lafayette, LA, USA

Key Points:

- Intra-ring $\delta^{18}O$ profiles were analyzed on three longleaf pine trees for the years 2001–2008 from the Louisiana Gulf Coast
- The $\delta^{18}O$ profile patterns were differentiated into two groups (wet vs. dry years) using unsupervised learning techniques
- Wet years produce asymmetrical profiles with persistently lower latewood $\delta^{18}O$ values

Supporting Information:

Supporting Information may be found in the online version of this article.

Correspondence to:

W. E. Lukens,
lukenswe@jmu.edu

Citation:

Lukens, W. E., Narmour, R. T., & Schubert, B. A. (2021). Seasonal hydroclimate recorded in high resolution $\delta^{18}O$ profiles across *Pinus palustris* growth rings. *Journal of Geophysical Research: Biogeosciences*, *126*, e2021JG006505. https://doi.org/10.1029/2021JG006505

Received 21 JUN 2021
Accepted 18 NOV 2021

Author Contributions:

Conceptualization: William E. Lukens, Robert T. Narmour, Brian A. Schubert
Data curation: William E. Lukens
Formal analysis: William E. Lukens, Robert T. Narmour, Brian A. Schubert
Funding acquisition: William E. Lukens, Brian A. Schubert
Investigation: William E. Lukens, Robert T. Narmour, Brian A. Schubert
Methodology: William E. Lukens, Robert T. Narmour, Brian A. Schubert
Project Administration: William E. Lukens, Brian A. Schubert
Resources: Brian A. Schubert
Supervision: William E. Lukens, Brian A. Schubert
Validation: William E. Lukens, Brian A. Schubert
Visualization: William E. Lukens

Abstract Rainfall amount and intensity are increasing under anthropogenic climate change, but many instrument records span less than a century. The oxygen isotopic composition of tree-ring cellulose ($\delta^{18}O_{cell}$) reflects local source water, climate, and tree physiology. The patterns of $\delta^{18}O_{cell}$ within tree-rings has the potential to extend pre-instrument climate records with subannual resolution, but the influences on intra-ring $\delta^{18}O_{cell}$ profiles are unexplored in many settings. In this study, high-resolution $\delta^{18}O_{cell}$ profiles were analyzed on three longleaf pine trees growing in a native savanna in Louisiana, United States. The time series covers a wide range of rainfall conditions from 2001 to 2008 C.E. with a total of 421 $\delta^{18}O_{cell}$ analyses. The $\delta^{18}O_{cell}$ values for individual years are well correlated with each other both within and between trees ($r = 0.71$–0.78). We used principal components analysis and *k*-means clustering to differentiate $\delta^{18}O_{cell}$ profiles into two groupings: symmetrical $\delta^{18}O_{cell}$ profiles versus asymmetrical profiles that have depressed latewood $\delta^{18}O_{cell}$ values. The slope of latewood $\delta^{18}O_{cell}$ profiles and mean $\delta^{18}O_{cell}$ values of latewood tissue correlate with total June-November precipitation. We hypothesize that poorly drained soils in the study area mediate the influence of any individual storm event: in dry years, ^{18}O-depleted signals from convective storms are moderated by subsequent evaporative enrichment of standing water, whereas in wet years, increased humidity and frequent re-supply of ^{18}O-depleted water overrides evaporative enrichment effects, resulting in low $\delta^{18}O_{cell}$ of latewood. These results suggest that $\delta^{18}O_{cell}$ proxies for tropical storm occurrence need to account for soil conditions at the site of tree growth.

Plain Language Summary Anthropogenic climate change is driving an increase in the amount and intensity of rainfall in many areas of the world. However, limited historical weather station records inhibit our ability to place these trends into a longer temporal context. Stable isotopes in tree-ring tissue can record local climate conditions as the tree grows; thus, analysis of wood samples along individual growth rings can provide high-resolution information on local weather conditions. Previous work used average values of oxygen isotopes from tree-rings to produce annual-average climate estimates or to identify years that recorded tropical storm occurrences near the site of growth. This study reports the first analyses of oxygen isotope time series measured within tree-rings from pine trees living in the Gulf Coast region of the United States. The isotope profiles within each ring showed one of two distinctive patterns: "L" shaped profiles reflect summer/autumn seasons with greater rainfall, whereas "U" shaped profiles reflect drier summer/autumn seasons. Our approach allows us to conclude that the isotope profiles likely record seasonal rainfall totals rather than the occurrence of individual storms (such as hurricanes). We suggest that poorly drained soils in the study area may prevent recording of tropical cyclones.

1. Introduction

Anthropogenic climate change is forcing a change in the characteristics of seasonal climate and extreme events (e.g., Easterling et al., 2017; Roque-Malo & Kumar, 2017), but understanding the magnitude and context of these trends is inhibited by relatively short instrument records in many regions of the world. The southeastern United States is likely to experience an increase in total annual rainfall in the coming decades, primarily driven by more intense and more frequent heavy rain events (Brown et al., 2019; Dourte et al., 2015; Moustakis et al., 2021); however, instrument records prior to the twentieth century are rare in the region, highlighting the need for longer chronologies of seasonal hydroclimate. The stable oxygen isotope composition of tree-ring cellulose ($\delta^{18}O_{cell}$) records climatic, environmental, and tree physiological conditions as a tree grows. Thus, subsampling yearly growth rings provides a substrate on which to develop intra-annual climatic and environmental proxy records. Time series of $\delta^{18}O_{cell}$ values have the potential to extend climate archives beyond the instrument record with high

Writing – original draft: William E. Lukens, Robert T. Narmour
Writing – review & editing: William E. Lukens, Brian A. Schubert

spatial and temporal resolution (Labotka et al., 2016; Managave et al., 2020; Qin et al., 2015; S. Shi et al., 2020; Treydte et al., 2007; Xu et al., 2018), and could also be applied on deep-time paleoclimate archives using fossil wood (Hook et al., 2014; Jahren & Sternberg, 2008; Richter, Johnson, Dranoff, LePage, & Williams, 2008; Schubert & Jahren, 2015).

The ultimate source of oxygen within tree-ring cellulose is meteoric water. The oxygen isotopic value of meteoric water ($\delta^{18}O_{MW}$) is highly correlated with various climate parameters (e.g., temperature: Dansgaard, 1964; moisture source: Araguás-Araguás et al., 1998; precipitation: Vachon et al., 2007; humidity: Kahmen et al., 2011) on local, regional, and global scales, providing a basis for paleoclimate reconstructions. Cellulose is enriched in ^{18}O relative to meteoric water because transpiration leads to evaporative enrichment of ^{18}O relative to ^{16}O within the leaf, and is further enriched by ∼27‰ due to isotopic exchange during cellulose synthesis (Roden et al., 2000; F. Shi et al., 2019; Sternberg, 2009). This leads to $\delta^{18}O_{cell}$ values being significantly greater than that of meteoric water, with large total offsets between $\delta^{18}O_{cell}$ and $\delta^{18}O_{MW}$ across individual sites and species (e.g., 35–44‰) (Jahren & Sternberg, 2002; Richter, Johnson, Dranoff, & Taylor, 2008). However, a global data set of *intra-annual* $\delta^{18}O_{MW}$ and $\delta^{18}O_{cell}$ data revealed a constant slope = 0.66 between $\delta^{18}O_{cell}$ and $\delta^{18}O_{MW}$ ($R^2 = 0.72$), suggesting that intra-ring cellulose profiles can be used to estimate sub-annual change in $\delta^{18}O_{MW}$ caused by seasonal climate (Schubert & Jahren, 2015).

The climatic information resolvable from $\delta^{18}O_{cell}$ analyses is dependent on both locality and sampling resolution. The majority of prior work focused on locally calibrated relationships between climate conditions and annual average $\delta^{18}O_{cell}$ values from whole-ring sampling, producing reconstructions of temperature (Huang et al., 2019; Loader et al., 2010), relative humidity (Grießinger et al., 2017; Jahren & Sternberg, 2003), and precipitation pattern (Brienen et al., 2013; Brunello et al., 2019; Managave et al., 2020; Sano et al., 2010). Analysis of the seasonal components of tree-ring tissue—earlywood and latewood—has produced records of seasonal precipitation source and amount (Labotka et al., 2016) and tropical storm occurrence (Altman et al., 2021; Lewis et al., 2011; Miller et al., 2006; Mora et al., 2007). Alternative approaches include subsampling growth rings at finer resolutions (sub-millimeter), producing $\delta^{18}O_{cell}$ profiles that capture sub-monthly to approximately weekly temporal resolution during the growing season (Li et al., 2011; Schollaen et al., 2013; Verheyden et al., 2004; Xu et al., 2016). The controls on high-resolution $\delta^{18}O_{cell}$ profile shape remains largely unexplored due to the substantial burden of sample preparation, with current hypotheses indicating the potential for resolving individual storm events (Li et al., 2011) and elucidating changes in source water composition and hydroclimatic conditions (Berkelhammer et al., 2020; Schollaen et al., 2013). Due to the relative paucity of intra-ring $\delta^{18}O_{cell}$ profile studies, the linkage between intra-ring $\delta^{18}O_{cell}$ patterns and sub-annual climatic conditions—including tropical storm occurrence—remains poorly understood, and replication of intra-ring $\delta^{18}O_{cell}$ profiles has yet to be tested within and between trees.

In this study, we investigated coeval $\delta^{18}O_{cell}$ profiles from three longleaf pine trees (*Pinus palustris* Mill.) growing in the native savanna biome of southwestern Louisiana (Figure 1). Our goals were to investigate the drivers of sub-annual $\delta^{18}O_{cell}$ patterns in a region that is particularly prone to tropical cyclone activity (Figures 1 and 2), but where intra-ring $\delta^{18}O_{cell}$ chronologies have yet to be studied. We hypothesized that high levels of precipitation during latewood growth (June-November) delivered meteoric water depleted in ^{18}O, thereby driving down latewood $\delta^{18}O_{cell}$ values via the "amount effect" (i.e., the amount of rainfall correlates negatively with the $\delta^{18}O$ value of rainfall, after Dansgaard, 1964). Thus, if the intra-ring $\delta^{18}O_{cell}$ profiles predominantly reflect seasonal hydroclimatic conditions, the slope of $\delta^{18}O_{cell}$ values in the latewood should be a predictor of $\delta^{18}O_{cell}$ profile shape. In contrast, if individual storm events were the driving mechanism behind latewood $\delta^{18}O_{cell}$ values, we would predict that short-lived, negative excursions in $\delta^{18}O_{cell}$ profiles would be evident, creating a highly variable $\delta^{18}O_{cell}$ profile pattern coincident with the occurrence of tropical storms and extreme rain events. To test these hypotheses, we applied unsupervised learning techniques (cluster and principal components analysis) to objectively differentiate $\delta^{18}O_{cell}$ profiles, which eliminates the need for subjective pattern recognition practices and allows for more clear understanding of climate-$\delta^{18}O_{cell}$ signal generation. We then applied regression analysis to test for associations between $\delta^{18}O_{cell}$ profile patterns and meteorological data from a nearby weather station.

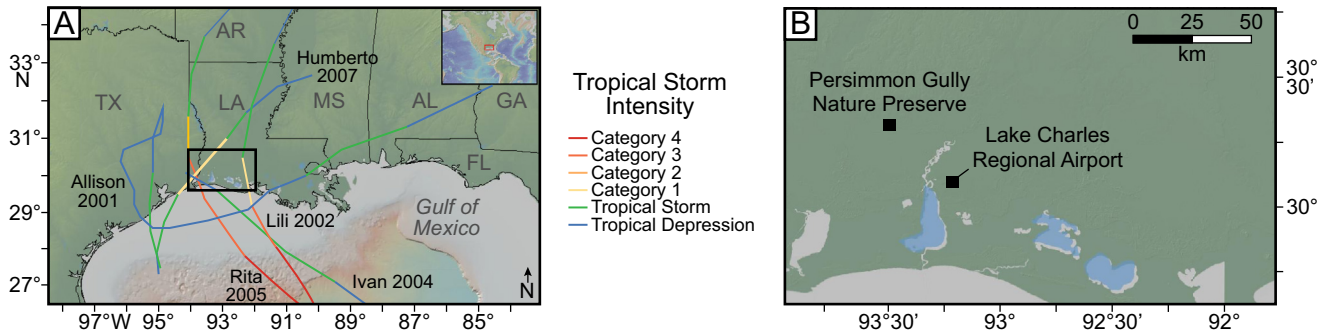

Figure 1. The study area is located in North America (a, inset) in southwest Louisiana; black box indicates area in panel b. Tropical storm tracks within 150 km of the study site are shown for the study period (years 2001–2008), with Saffir-Simpson storm intensity indicated (redrawn from https://coast.noaa.gov/hurricanes/). Gray letters refer to state name abbreviations. (b) Longleaf pine cores were collected at the Persimmon Gully Nature Preserve. Meteorological records were queried from the Global Historical Climatological Network from the Lake Charles Regional Airport station. Base maps were generated with GeoMapApp (www.geomapapp.org).

2. Materials and Methods

2.1. Site Description

The trees sampled in this study are growing at the Persimmon Gully Nature Preserve (30° 19' N, 93° 32' W, 15 masl) in southwestern Louisiana (Figure 1). Soils in the study area are predominantly Brimstone Silt Loam (fine-silty, siliceous, superactive, and thermic Glossic Natraqualfs) that occur on fluviomarine deposits with high exchangeable sodium, poor drainage and slow permeability (Roy & Midkiff, 1988). Persimmon Gully is dominated by old-growth longleaf pines (*Pinus palustris* Mill.), and to a lesser extent, loblolly pines (*Pinus taeda* L.). Four cores (2A, 3B, 15A, 15B; all *Pinus palustris*) were extracted from three longleaf pine trees using an increment

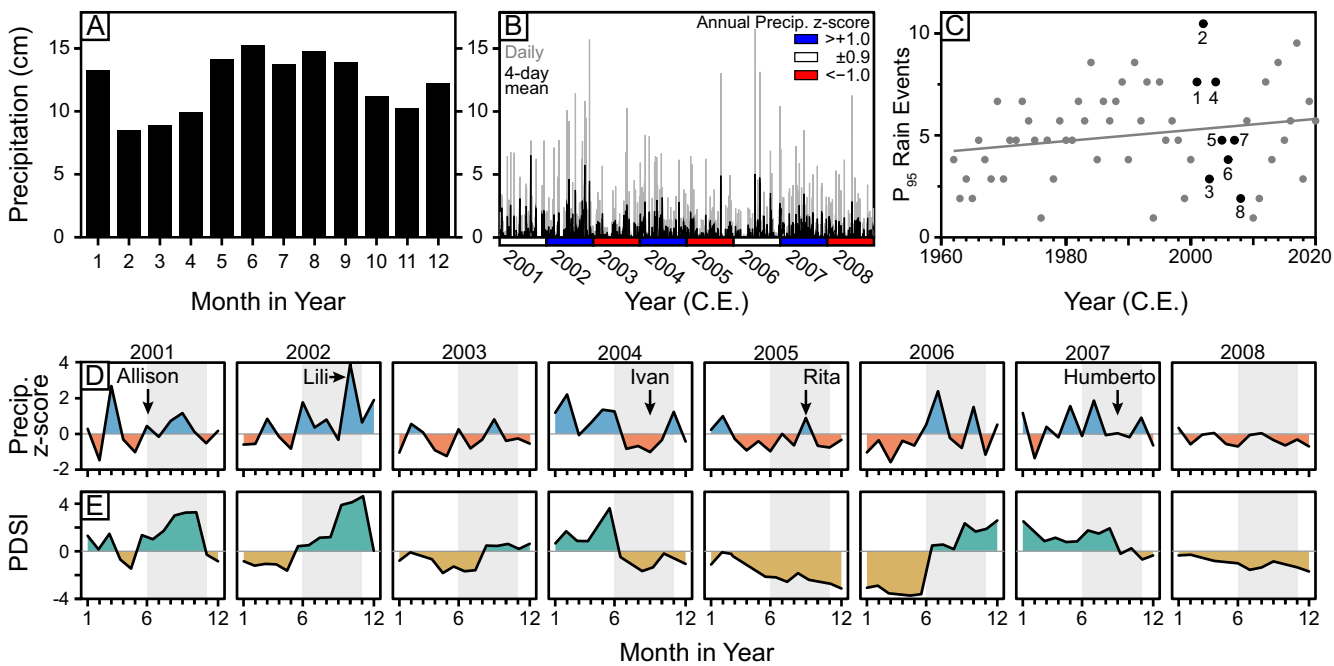

Figure 2. Hydroclimate of Persimmon Gully, southwest Louisana. (a) Mean monthly precipitation (1962–2020 C.E.). (b) Daily precipitation totals for the study interval. Each year is color coded according to the *z*-score of annual precipitation, standardized to 1962–2010 C.E. (c) Number of days with rainfall totals surpassing the 95th percentile (P_{95} rain events). The slope of the linear regression is not significantly different from zero. Data points corresponding to the study interval are highlighted as black symbols annotated with the year in the study interval. (d) Monthly precipitation z-scores across the study interval, standardized to monthly values from 1962 to 2010 C.E. Tropical storm strikes within 150 km of the study area are indicated. (e) Palmer Draught Severity Index (PDSI) for southwest Louisiana (NOAA State 16, Division 7). Gray shading in panels d and e highlights June-November, coinciding with hurricane season and approximate interval of latewood growth in tree-rings. See text for data sources and calculation details.

borer. One tree was sampled in duplicate from opposite sides of the trunk to produce two replicate cores (15A and 15B) to study intra-tree replication of oxygen isotope profiles. The four cores were mounted on wooden bases and sanded with 600-grit sandpaper to aid in identification of annual growth rings. Annual rings were demarcated after observation of each core under an optical stereomicroscope.

2.2. Climate Setting

Daily and monthly meteorological data were queried from the Global Historical Climatology Network (GHCN) version 4 (Menne et al., 2018) for the Lake Charles Regional Airport (station ID: USW00003937; Figure 1). The GHCN-monthly data included precipitation totals and temperature averages for the years 1962–2020, whereas GHCN-daily data were limited to daily precipitation totals. Rainfall is relatively evenly distributed throughout the year at the study site, with slightly higher monthly totals in May-September (Figure 2a). Annual growth rings corresponding to the years 2001–2008 were targeted for this study because these years cover a wide range of annual precipitation: whereas the longterm (1962–2010) mean annual precipitation is 142.3 cm, the study interval varies from 111.6 cm (z-score = −1.1) to 216.5 cm (z-score = +2.6) (Figure 2b). Further, these years encompass a large range of extreme precipitation frequency, as measured by daily precipitation totals (Figure 2b) and P_{95} events (Figure 2c), the latter of which are calculated as daily non-zero totals that exceed the 95th percentile of the entire record (1962–2020, P_{95} = 5.38 cm; cf. Easterling et al., 2017).

Monthly precipitation z-scores were calculated for the study interval by standardizing monthly totals in the years 2001–2008 to the mean and standard deviation of GHCN-monthly records up to and including the decade of sampling (i.e., 1962–2010; Figure 2d). The study interval spans years that had higher and lower than average monthly rainfall, which generally correspond to monthly Palmer Drought Severity Index (PDSI; Palmer, 1965) for the study area (Division 7, www.ncdc.noaa.gov/cag/). PDSI values range from −4 (extreme drought) to +4 (extremely moist). Hurricane strikes within 150 km of the study area were compiled from storm tracks published by the NOAA National Hurricane Center Atlantic hurricane database (HURDAT2; https://coast.noaa.gov/hurricanes) (Figures 1 and 2).

2.3. Oxygen Isotope Analysis

Tree rings corresponding to the years 2001–2008 range in width from 0.6 to 3.5 mm. The rings were manually sampled at 0.1–0.3 mm resolution under a binocular microscope using a razor blade, resulting in an average of 14 slices per growth ring. Provided that the average growing season for pine trees in this area is approximately nine months (March to November; Kramer, 1943) this equates to an average of ∼2.8 weeks of growth per sample (assuming equal growth rates). This is of comparable resolution to other high-resolution studies of intra-ring $\delta^{18}O_{cell}$ (Berkelhammer et al., 2020; Li et al., 2011; Verheyden et al., 2004; Xu et al., 2016). Cellulose was extracted from a total of 421 bulk wood slices using the modified Brendel method (Brendel et al., 2000; Gaudinski et al., 2005). We chose this method because it reduces the burden of time and resources compared to the more widely used Jayme-Wise method (Green & Whistler, 1963; Leavitt & Danzer, 1993) while yielding comparable $\delta^{18}O_{cell}$ data (Gaudinski et al., 2005). Purified α-cellulose samples ranging in mass from approximately 50-100 µg were wrapped in silver capsules and analyzed for $\delta^{18}O_{cell}$ values using a High-Temperature Conversion Elemental Analyzer coupled with a DELTA V Advantage Isotope Ratio Mass Spectrometry (IRMS) instrument (Thermo Fisher Scientific, Inc., USA) located at the University of Louisiana at Lafayette. The resulting values were expressed in delta notation ($\delta^{18}O$) in units per mil (‰) with respect to reference Vienna standard mean ocean water (VSMOW):

$$\delta_{sample} = (R_{sample}/R_{standard} - 1)\ x\ 1000 \quad (1)$$

where R_{sample} and $R_{standard}$ are the molar ratios of $^{18}O/^{16}O$ in the samples and standards, respectively. Two internal laboratory standards (ACELL = 32.33 ± 0.06‰, JCELL01 = 17.64 ± 0.09‰) and a quality control sample (JCELL02 = 20.44‰) were analyzed with the cellulose samples. Standard deviation of the quality control samples was 0.11‰ (n = 9).

3. Data Preparation

3.1. Oxygen Isotope Data

We generated isotopic profiles standardized in two dimensions by calculating z-scores from measured $\delta^{18}O_{cell}$ values (y-axis) and by resampling the $\delta^{18}O_{cell}$ z-scores at regular intervals along normalized tree-ring widths (x-axis). The z-scores were calculated by subtracting each $\delta^{18}O_{cell}$ observation by the mean value of the ring and dividing by the standard deviation. Each $\delta^{18}O_{cell}$ z-score profile was then interpolated to a common resolution of 10 evenly spaced points using a smoothing spline drawn through each profile, followed by extraction of the z-score values at each of the 10 normalized intra-ring positions (after Berkelhammer et al., 2020). The first sample in each interpolated profile was set to be the first calculated z-score value for each ring, which corrected deviations between the splines and actual z-scores in the early zones of the rings. These transformations (z-scores and interpolations) together produced standardized patterns with identical resolution across all rings that contained clearly defined profiles, hereafter referred to as standardized profiles. The patterns of $\delta^{18}O_{cell}$ observations closely matched the standardized profiles without imparting any biases. Only rings with more than four intra-ring $\delta^{18}O_{cell}$ measurements were included in the analysis; two out of the 32 tree rings were therefore omitted from analysis due to low sample resolution—ring 8 (2008) from tree core 15A and ring 4 (2004) from tree core 2A.

3.2. Statistical Analysis

In order to objectively differentiate standardized $\delta^{18}O_{cell}$ profile shapes, we utilized a combination of principal components analysis (PCA) and k-means cluster analysis, which are two widely used tools in multivariate statistics and data analytics. This approach was specifically taken to mitigate the need for subjective pattern matching when analyzing the standardized profiles. PCA is an unsupervised learning technique that rescales and recenters input variables into a new reference frame, with the goal of maximizing variance in fewer dimensions than the raw, multivariate input data (Davis, 2002). The net result is a collapse of redundant information stored across multiple dimensions (here, tree-ring sampling positions), which allows one to identify the positions within the $\delta^{18}O_{cell}$ profiles that are unique between individual tree-rings. Principal components (PCs) are calculated as linear combinations of eigenvectors of the correlation matrix, with eigenvalues representing the variance of each PC. Each PC is orthogonal to all others, and the total number of PCs will equal the number of input dimensions. However, the transformations executed by PCA often result in the majority of variance in the data set being explained by the first few PCs, and therefore the other dimensions can be ignored as noise in the system (e.g., Borůvka et al., 2005; Lukens et al., 2018; Mandal et al., 2008). This approach is particularly useful for data sets with multiple correlative variables—by combining the information of these variables, trends in the multivariate data can be collapsed to lower dimensionality to reveal latent structures that were less clear initially. In this analysis, the input variables for PCA were the 10 evenly spaced positions in the standardized profiles, and the values for each of these variables are the $\delta^{18}O_{cell}$ z-scores at each interpolated position. The z-scores were centered and scaled prior to PCA, as their values and variances are not uniform across each ring profile or tree core.

Following PCA, the standardized $\delta^{18}O_{cell}$ profiles were assigned to groupings using k-means cluster analysis (Berkelhammer et al., 2020). The k-means algorithm divides samples into clusters by iteratively seeking to minimize the within-group sum of squares while maximizing the between-group sum of squares. In other words, this technique allows for objective differentiation of data sets into similar groupings using reproducible criteria. Clustering was initiated with 20 random starts. The number of clusters (k) can be subjective, but here was decided using the "elbow rule": the value of k is chosen where an increase in the number of clusters fails to appreciably reduce the within-group sum of squares (here, $k = 2$; see Section 4.3). As in PCA, the input variables for the k-means analysis were the $\delta^{18}O_{cell}$ z-scores at 10 interpolated positions in the tree-ring profiles, but the z-scores were not centered or scaled prior to k-means analysis. Taken together, the k-means cluster analysis divided the standardized profiles into two natural groupings, and the PCA demonstrates the characteristics of the profiles that lead to these differentiations.

All data analysis was performed in RStudio version 3.6.1 (R Core Team, 2020) using the following packages: tidyverse (Wickham et al., 2019), broom (Robinson et al., 2021), lubridate (Grolemund & Wickham, 2011), and factoextra (Kassambara & Mundt, 2020).

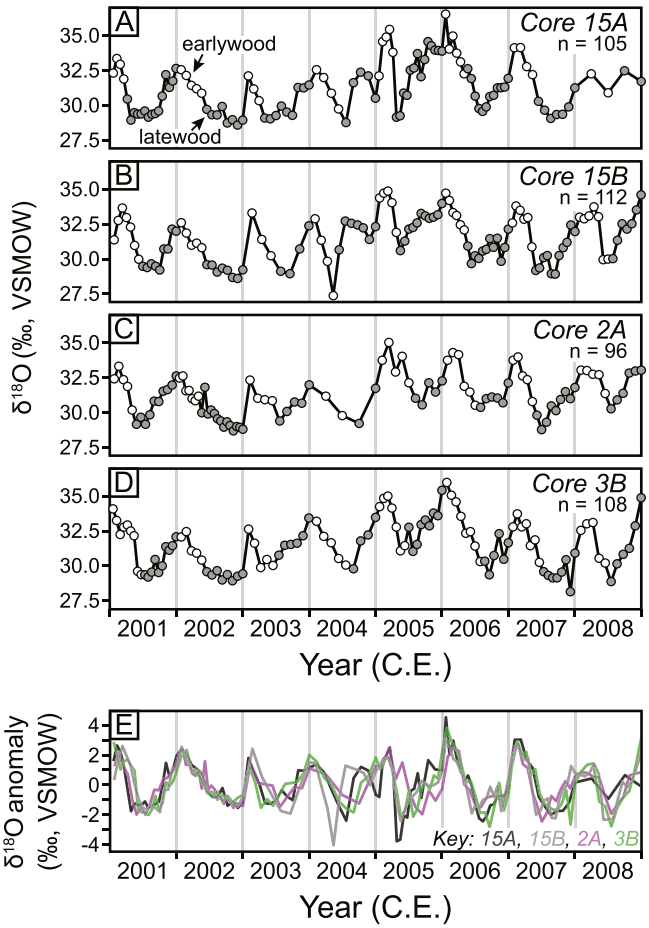

Figure 3. (a–d) Profiles of $\delta^{18}O_{cell}$ values across the *Pinus palustris* tree cores. Gray vertical lines indicate ring boundaries. White symbols are earlywood; gray symbols are latewood. Tree core code and number of analyses (*n*) per core are indicated in upper right of each panel. Note that cores 15A and 15B are replication cores from the same tree. (e) Stacked profiles of $\delta^{18}O_{cell}$ anomaly, calculated by subtracting mean $\delta^{18}O_{cell}$ of each ring from observed $\delta^{18}O_{cell}$ values.

4. Results

4.1. $\delta^{18}O_{cell}$ Profiles

The intra-ring $\delta^{18}O_{cell}$ profiles all show a similar pattern of high earlywood $\delta^{18}O_{cell}$ values at the start of each ring decreasing toward the center of the growth ring (Figure 3). Most rings show a pattern of $\delta^{18}O_{cell}$ maxima at the ring boundaries and minima near the transition to latewood (i.e., early to mid-summer). However, low $\delta^{18}O_{cell}$ values persist in some rings throughout the entire latewood interval (Figure 3). The $\delta^{18}O_{cell}$ values within individual rings vary by 4.4‰ on average (range = 1.6–7.0‰). Within latewood, $\delta^{18}O_{cell}$ values vary by 2.9‰ on average (range = 0.7–6.0‰).

Replication within and between trees was inspected by plotting $\delta^{18}O_{cell}$ anomalies, calculated by subtracting each $\delta^{18}O_{cell}$ observation from the mean $\delta^{18}O_{cell}$ value of the growth ring. These rescaled $\delta^{18}O_{cell}$ profiles overlap very well and therefore demonstrate that intra- and inter-annual $\delta^{18}O_{cell}$ patterns are recorded clearly within individual trees (cores 15A and 15B) and across trees (Figure 3). Linear correlation tests were analyzed on the standardized $\delta^{18}O_{cell}$ profiles, as standardization removed any secular trends in the time series and the interpolation yielded a common resolution across tree cores. The $\delta^{18}O_{cell}$ *z*-scores between cores have shown high correlation coefficients, ranging from 0.71 to 0.80, with all correlations being significant (Pearson's correlation test; $p < 0.001$ for each comparison; Table 1).

4.2. Principal Components Analysis

The PCA resulted in two PCs that explain a total of 66.7% of the total variance (Figures 4a and 4b). The variable loadings on PC1 are oriented such that positive PC1 values are associated with the first five positions, whereas negative PC1 values are associated with the last four positions in each ring. PC1 therefore separates the first and second half of each standardized profile: rings with high scores on PC1 have high z-scores in the first half of the ring and low z-scores in the latter half of the ring. The standardized profiles and the relative contribution of each dimension (tree-ring position) in generating PCs is shown in Figures 4c–4e. The last three ring positions (i.e., the latest intervals of growth in each year) contribute the most toward PC1. The contribution of the first five positions to PC1 is likely an artifact of the z-score transformation, as all $\delta^{18}O_{cell}$ profiles show descending values at the beginning of each ring. Positions at the center of the tree-rings contribute very little toward PC1, as the z-scores are generally similar at position 6 across all rings.

PC2 is oriented orthogonal to PC1, and therefore does not contain information on the overall shape of profiles. PC2 seems to be identifying variability in the middle of the rings due to a few anomalous rings that have minima

Table 1
Pairwise Correlation Tests Between Standardized $\delta^{18}O_{cell}$ Profiles

Tree core	15A	15B	2A	3B
15A	–			
15B	0.71 (0.56, 0.81)	–		
2A	0.73 (0.58, 0.83)	0.73 (0.60, 0.83)	–	
3B	0.80 (0.70, 0.87)	0.72 (0.59, 0.81)	0.75 (0.63, 0.84)	–

Note. All results show Pearson's correlation coefficient (*r*) with the 95% confidence interval about the estimate of *r* in parentheses. All models are significant with $p < 0.001$.

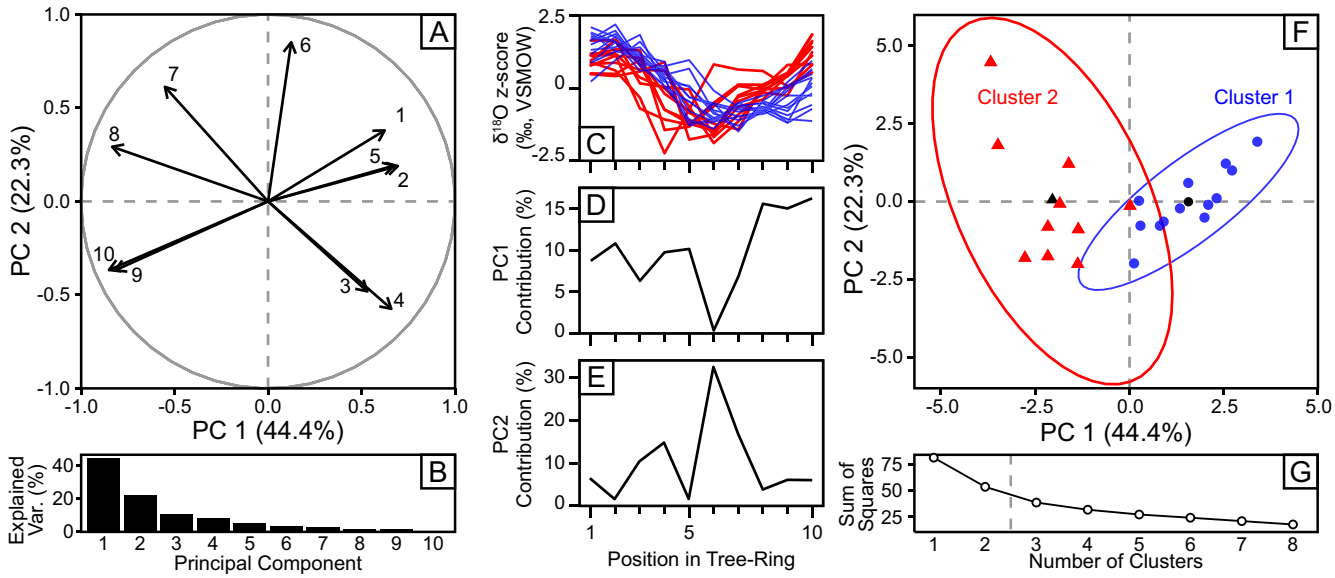

Figure 4. Principal components (PC) and *k*-means cluster analysis results. (a) Variable loading plot on PCs 1 and 2. Numbers refer to order of *z*-score value within tree-rings. (b) Scree plot showing percent of explained variance by each PC. The first two PCs capture 66.7% of the total variance. (c) Interpolated $\delta^{18}O$ z-scores for all rings within the analysis (cores 15B, 2A, and 3B). Colors are coded to *k*-means clusters (box F). Cluster 1 (blue) are designated as "event" years and cluster 2 (red) are normal years. (d and e) Contribution (in percent) of each ring position toward generating PC 1 (d) and PC 2 (e). (f) *K*-means cluster designations for each ring projected into PC space for $k = 2$ clusters. Black symbols are the centroids of each cluster; ellipses are the 95% probabilities about each centroid. (g) Scree plot of cluster number (k) indicating that more than two clusters results in diminishing returns in decreasing the within-group sum of squares.

early in the ring, and therefore recover to higher z-score values by the middle of the ring. The PC scree plot indicates that PCs 3–10 individually explain relatively little variance and are not discussed here (Figure 4b).

4.3. Cluster Analysis

The *k*-means results are shown in Figures 4f and 4g. Clusters 1 and 2 are clearly separated along PC1, which indicates that the differences in overall profile shape (*z*-score value early and late in each ring) is the mechanism used to separate rings. The within-group sum of squares decreases rapidly for any number of clusters (*k*) above 2, therefore analysis with $k > 2$ would be inappropriate here. The observations within both clusters overlap along PC2, further supporting the inference that PC2 is not related to profile shape. The 95% probability envelopes about the centroids of each cluster envelop a small number of samples between the two clusters. Cluster assignments for each of the individual profiles is shown in Figure 5.

5. Discussion

The $\delta^{18}O_{cell}$ profiles from the longleaf pine tree-rings are well correlated both within and between trees at Persimmon Gully. This observation demonstrates that the trees are recording a common and reproducible response to local environmental conditions. Tree-rings corresponding to the years 2001–2008 coincide with five direct hurricane strikes in southwest Louisiana (Figures 1a and 2d), yet we did not observe a robust tempestological signal across the three trees analyzed in this study. We instead suggest that the $\delta^{18}O_{cell}$ profile patterns reflect seasonal average hydroclimatic conditions mediated by soil water residence time.

The PCA and *k*-means analyses differentiated the $\delta^{18}O_{cell}$ profiles into two groups: (a) rings that have latewood $\delta^{18}O_{cell}$ values similar to that of earlywood, creating a "U" shape across the growth ring (Cluster 1: coded as blue in Figures 4–6); and (b) rings that retain low $\delta^{18}O_{cell}$ values across the latewood growth interval, creating an "L" shaped profile (Cluster 2: coded as red in Figures 4–6). The *k*-means cluster assignments were fully consistent across the three individual trees for four of the eight years included in this study (Figures 4 and 5), and a fifth year (2004) had a consensus between the two rings included in the analysis. The other three years (2001, 2003, and

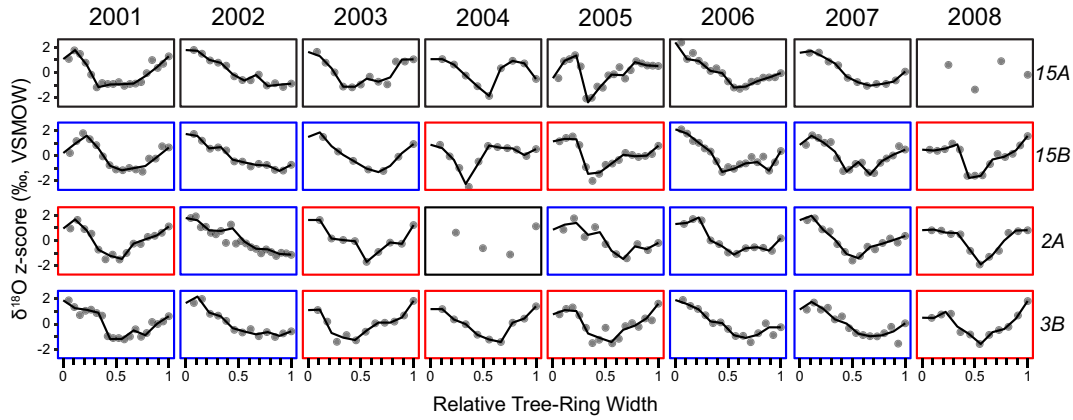

Figure 5. Profiles of measured $\delta^{18}O_{cell}$ values (gray symbols; plotted as z-scores) and interpolated $\delta^{18}O_{cell}$ profiles using a smoothing spline (black lines). Outlines of each plot indicate the cluster assignment from *k*-means analysis: blue = Cluster 1 = "L" pattern, red = Cluster 2 = "U" pattern, black = not included in *k*-means analysis. Tree cores (rows) are labeled on the ride side of the figure; columns are aligned by calendar year (C.E.).

2005) had mixed cluster assignments between the trees, possibly due to varying growth rates that shifted $\delta^{18}O_{cell}$ minima across the normalized tree-ring widths.

We hypothesized that seasonal precipitation totals were the driver of $\delta^{18}O_{cell}$ profile shape. To test this, we calculated linear regression models for the latewood portion of each $\delta^{18}O_{cell}$ profile:

$$\delta^{18}O_{cell} = m_{LW} \times D + b \quad (2)$$

where D is the normalized distance across each tree-ring, m_{LW} is the slope of the linear fit, and b is the y-intercept. We found a significant, negative relationship between June-November precipitation and m_{LW} (Figure 6a): rings with higher rainfall during the interval coincident with latewood growth showed either negative or relatively flat slopes (i.e., 2002, 2006, 2007), whereas years with lower June-November rainfall totals coincide with the symmetrical, "U-shaped" $\delta^{18}O_{cell}$ profiles that have higher m_{LW} values (i.e., 2001, 2003, 2004, 2005, 2008). This linear relationship is significant across all individual trees (Figure 6), but is improved when m_{LW} is averaged between trees (Table S1 in Supporting Information S1). The overall trend of decreasing m_{LW} with higher June-November

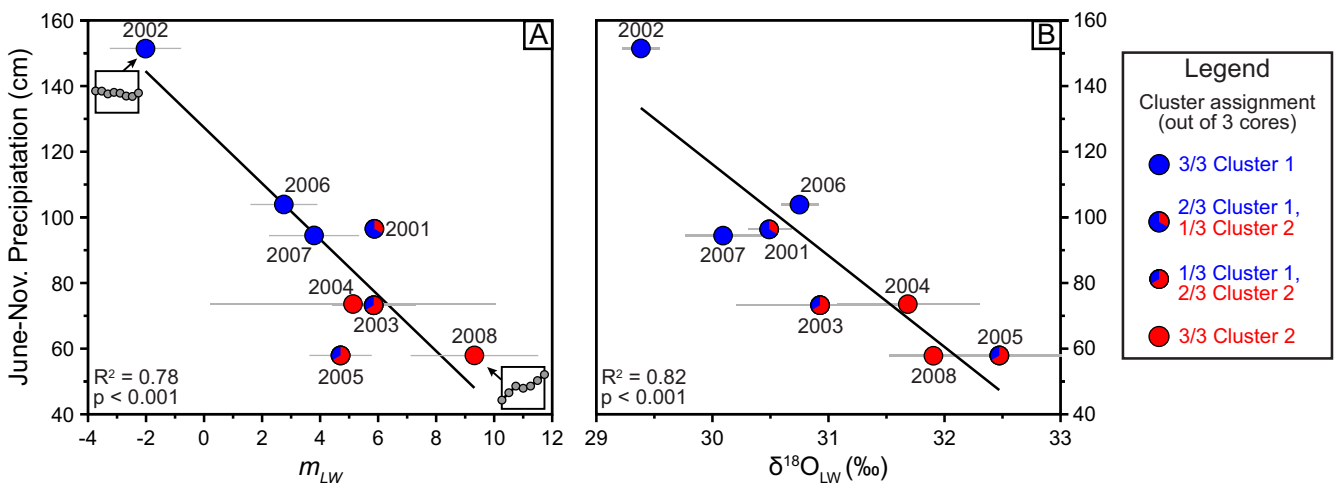

Figure 6. Total precipitation during hurricane season (June–November) versus (a) the intra-ring slope of $\delta^{18}O_{cell}$ values in latewood (m_{LW}), and (b) the weighted mean of latewood $\delta^{18}O_{cell}$ values ($\delta^{18}O_{LW}$). Linear regressions were calculated for mean values of the dependent (*x*-axis) variable using data for all rings in the cores 15B, 2A, and 3B. Gray bars indicate standard deviation between cores. Shading of symbols indicates the proportion of trees that are assigned as Cluster 1 (blue) or Cluster 2 (red) for each year. Example rings from core 15B are shown in A for the years 2002 and 2008, with latewood shown as dark gray symbols (insets; see Figure 3b). The units for m_{LW} are in ‰ per unitless (normalized) distance. See Table S1 for regression metrics across individual trees and the main text for details of regression analysis.

rainfall matches well with the classification of $\delta^{18}O_{cell}$ profiles into Cluster 1 (wetter/lower m_{LW}) versus Cluster 2 (drier/higher m_{LW}). From this we conclude that individual storm events are not the primary control on $\delta^{18}O_{cell}$ profiles at the study site.

Why do the $\delta^{18}O_{cell}$ profiles at Persimmon Gully reflect seasonally integrated hydroclimate signals? Here we pose two possible explanations to this question. First, the soils in the study area are poorly drained, fine-grained, and occur on level slopes (Roy & Midkiff, 1988). The low slope and permeability cause water to pool during storm events (Roy & Midkiff, 1988), which would lengthen the residence time of soil water derived from individual storms and promote mixing with water from subsequent storms. In abnormally wet summer and fall seasons (e.g., 2002), the soils would have been continuously saturated with precipitation, which would have decreased evaporative enrichment (due to increased relative humidity). Repeated precipitation events in these wet years delivered ^{18}O-depleted source water during latewood tissue generation. Conversely, during a dry year (e.g., 2005), precipitation that fell from individual storms (e.g., Hurricane Rita) would have undergone evaporative enrichment as it slowly percolated through soil profiles, and any ^{18}O-depleted precipitation produced from this hurricane would be masked by the time it was taken up by the trees. These inferences support the results of Lewis et al. (2011), who found that the latewood $\delta^{18}O_{cell}$ anomaly method for detecting tropical storm strikes was less effective during drought years (i.e., 2005) in southeast Texas. For example, Hurricane Rita produced 13 cm of precipitation in less than a day in Lake Charles, but the records from 2005 contain some of the most enriched $\delta^{18}O_{cell}$ values in the time series of this study due to the dry conditions before and after the storm (Figure 2e).

A second possible explanation for the lack of tropical storm signals in the $\delta^{18}O_{cell}$ records at Persimmon Gully is that intense, convective precipitation events are relatively common in the Gulf Coast region and are not limited to tropical storms. For example, precipitation totals from Hurricane Lili on 3 October 2002 were 6.2 cm at the Lake Charles Regional Airport (LCRA) weather station. An upper level trough stalled in the area later that month between October 25 and 29 and delivered 27.5 cm of rain in just five days (National Weather Service, weather.gov/lch/events) (Figure 2b). In 2005, southwest Louisiana was under extreme drought conditions until Hurricane Rita delivered 19.5 cm of rain in two days (Figure 2e). Drought conditions returned and worsened until October of 2006, when strong storm systems from the Gulf of Mexico resulted in 20.9 cm of rain falling in just five days (October 15-19), causing serious flooding. These examples highlight the fact that tropical cyclones are not the only type of system that delivers major rainfall along the Gulf Coast, which dampens the signal of hurricanes in the longleaf pine $\delta^{18}O_{cell}$ records where soils are poorly drained and $\delta^{18}O_{MW}$ signals of tropical storms can be overridden by subsequent evaporative enrichment.

A number of studies have correlated average latewood $\delta^{18}O_{cell}$ values to hurricane activity in the past (Altman et al., 2021; Lewis et al., 2011; Miller et al., 2006), while others have linked these values to the amount of precipitation and relative humidity (Cai et al., 2018; Danis et al., 2006; Managave et al., 2011; S. Shi et al., 2020; Xu et al., 2015, 2018; Yang et al., 2021). Clearly, the magnitude and style of climate-$\delta^{18}O_{cell}$ signal expression in any tree-ring chronology is dependent on local conditions and climate setting. High-resolution, intra-ring $\delta^{18}O_{cell}$ analysis offers a means to examine the temporal architecture of $\delta^{18}O_{cell}$ signal generation—in some cases, low bulk $\delta^{18}O_{cell}$ values may be due to short-lived excursions in $\delta^{18}O_{cell}$ over timespans equivalent to days or weeks, whereas others may result from protracted intervals (months) of depressed $\delta^{18}O_{cell}$ values. The intra-ring $\delta^{18}O_{cell}$ patterns shown in this study suggest that depletion of $\delta^{18}O_{cell}$ values persisted for months in each wet year; thus, future work may benefit from studying at least a subset of intra-ring $\delta^{18}O_{cell}$ profiles in order to maximize explanatory power in new $\delta^{18}O_{cell}$ chronologies. Our hypotheses related to seasonal precipitation amount as the dominant control on $\delta^{18}O_{cell}$ profile pattern should be tested in future work to further elucidate other possible climatic drivers of $\delta^{18}O_{cell}$ profile pattern, namely temperature and relative humidity. We note that on average, June-November rainfall explains roughly 80% of the variation in both latewood slope (m_{LW}) and average latewood $\delta^{18}O_{cell}$ value ($\delta^{18}O_{LW}$), leaving unexplained at least 20% of the variation in $\delta^{18}O_{cell}$ profile patterns. Finally, our inference that soil properties may be an important mediator between $\delta^{18}O_{cell}$ and the resolution of rain events recorded in tree-rings suggests that researchers should be cautious when studying *ex situ* subfossil wood with unknown provenance.

6. Conclusions

This study developed high-resolution, intra-ring $\delta^{18}O_{cell}$ profiles from *P. palustris* on the Louisiana Gulf Coast to investigate the drivers of latewood $\delta^{18}O_{cell}$ signals. The $\delta^{18}O_{cell}$ profiles were reproducible both within and between trees. The shape of $\delta^{18}O_{cell}$ profiles was found to be governed by seasonal hydroclimate, namely the total precipitation throughout the summer to autumn, and did not show a reproducible signal of the "amount effect" within the $\delta^{18}O_{cell}$ profiles caused by individual tropical cyclones or extreme rainfall events. We hypothesize that poorly drained soils in the study area mediate the influence of any individual storm event: in dry years, signals of ^{18}O-depleted water delivered from convective storms are moderated by subsequent evaporative enrichment of the standing water, whereas in wet years, increased humidity and frequent re-supply of ^{18}O-depleted water overrides the effect of evaporative enrichment, resulting in low $\delta^{18}O_{cell}$ of latewood.

Data Availability Statement

The Global Historical Climatology Network (GHCN) data sets for Lake Charles, LA, are available at: https://www.ncdc.noaa.gov/ghcnd-data-access (GHCN-daily), https://www.ncdc.noaa.gov/data-access/land-based-station-data/land-based-datasets/global-historical-climatology-network-monthly-version-4 (GHCN-monthly). Data generated in this project are available in the Pangaea data repository at: https://doi.org/10.1594/PANGAEA.936601.

Acknowledgments
The authors thank Yingfeng Xu for laboratory assistance and Tom Doyle for assistance with field collections and cross-dating of the tree cores. Site access was provided by Latimore Smith, Richard Jacob, and Richard Martin of the Nature Conservancy. Funding for this project was provided by the U.S. National Science Foundation (grant no. AGS-1903601) and subaward grant #330175-01 from the University of Louisiana at Lafayette.

References

Altman, J., Saurer, M., Dolezal, J., Maredova, N., Song, J.-S., Ho, C.-H., & Treydte, K. (2021). Large volcanic eruptions reduce landfalling tropical cyclone activity: Evidence from tree rings. *Science of the Total Environment*, *775*, 145899. https://doi.org/10.1016/j.scitotenv.2021.145899

Araguás-Araguás, L., Froehlich, K., & Rozanski, K. (1998). Stable isotope composition of precipitation over Southeast Asia. *Journal of Geophysical Researc*, *103*, 28721–28742. https://doi.org/10.1029/98JD02582

Berkelhammer, M., Still, C. J., Ritter, F., Winnick, M., Anderson, L., Carroll, R., et al. (2020). Persistence and plasticity in conifer water-use strategies. *Journal of Geophysical Research: Biogeosciences*, *125*. https://doi.org/10.1029/2018JG004845

Borůvka, L., Vacek, O., & Jehlička, J. (2005). Principal component analysis as a tool to indicate the origin of potentially toxic elements in soils. *Geoderma*, *128*, 289–300.

Brendel, O., Iannetta, P. P. M., & Stewart, D. (2000). A rapid and simple method to isolate pure alpha-cellulose: Phytochemical Analysis. *An International Journal of Plant Chemical and Biochemical Techniques*, *11*, 7–10. https://doi.org/10.1002/(sici)1099-1565(200001/02)11:1<7::aid-pca488>3.0.co;2-u

Brienen, R. J. W., Hietz, P., Wanek, W., & Gloor, M. (2013). Oxygen isotopes in tree rings record variation in precipitation $\delta^{18}O$ and amount effects in the south of Mexico: Oxygen isotopes in tree rings. *Journal of Geophysical Research: Biogeosciences*, *118*, 1604–1615. https://doi.org/10.1002/2013JG002304

Brown, V. M., Keim, B. D., & Black, A. W. (2019). Climatology and trends in hourly precipitation for the southeast United States. *Journal of Hydrometeorology*, *20*, 1737–1755. https://doi.org/10.1175/jhm-d-19-0004.1

Brunello, C. F., Andermann, C., Helle, G., Comiti, F., Tonon, G., Tiwari, A., & Hovius, N. (2019). Hydroclimatic seasonality recorded by tree ring δ18O signature across a Himalayan altitudinal transect. *Earth and Planetary Science Letters*, *518*, 148–159. https://doi.org/10.1016/j.epsl.2019.04.030

Cai, Q., Liu, Y., Duan, B., Li, Q., Sun, C., & Wang, L. (2018). Tree-ring δ18O, a tool to crack the paleo-hydroclimatic code in subtropical China. *Quaternary International*, *487*, 3–11. https://doi.org/10.1016/j.quaint.2017.10.038

Danis, P. A., Masson-Delmotte, V., Stievenard, M., Guillemin, M. T., Daux, V., Naveau, P., & von Grafenstein, U. (2006). Reconstruction of past precipitation δ18O using tree-ring cellulose δ18O and δ13C: A calibration study near Lac d'Annecy, France. *Earth and Planetary Science Letters*, *243*, 439–448. https://doi.org/10.1016/j.epsl.2006.01.023

Dansgaard, W. (1964). Stable isotopes in precipitation. *Tellus*, *16*, 436–468. https://doi.org/10.3402/tellusa.v16i4.8993

Davis, J. C. (2002). *Statistics and data analysis in geology* (p. 656). New York: Wiley.

Dourte, D. R., Fraisse, C. W., & Bartels, W.-L. (2015). Exploring changes in rainfall intensity and seasonal variability in the Southeastern US: Stakeholder engagement, observations, and adaptation. *Climate Risk Management*, *7*, 11–19. https://doi.org/10.1016/j.crm.2015.02.001

Easterling, D. R., Arnold, J., Knutson, T., Kunkel, K., LeGrande, A., Leung, L. R., et al. (2017). Precipitation change in the United States, Washington, D.C., U.S. In *Climate Science Special Report: Fourth National Climate Assessment* (Vol. 1, pp. 207–230). Global Change Research Program.

Gaudinski, J. B., Dawson, T. E., Quideau, S., Schuur, E. A. G., Roden, J. S., Trumbore, S. E., et al. (2005). Comparative Analysis of Cellulose Preparation Techniques for Use with 13C, 14C, and 18O Isotopic Measurements. *Analytical Chemistry*, *77*, 7212–7224. https://doi.org/10.1021/ac050548u

Green, J. W., & Whistler, R. L. (1963) (Eds.), *Methods of carbohydrate chemistry* (p. 10).

Grießinger, J., Bräuning, A., Helle, G., Hochreuther, P., & Schleser, G. (2017). Late Holocene relative humidity history on the southeastern Tibetan plateau inferred from a tree-ring δ18O record: Recent decrease and conditions during the last 1500 years. *Quaternary International*, *430*, 52–59. https://doi.org/10.1016/j.quaint.2016.02.011

Grolemund, G., & Wickham, H. (2011). Dates and times made easy with lubridate. *Journal of Statistical Software*, *40*, 1–25. https://doi.org/10.18637/jss.v040.i03

Hook, B. A., Halfar, J., Gedalof, Z., Bollmann, J., & Schulze, D. (2014). Stable isotope paleoclimatology of the earliest Eocene using kimberlite-hosted mummified wood from the Canadian Subarctic. *Biogeosciences Discussions*, *11*.

Huang, R. (2019). Temperature signals in tree-ring oxygen isotope series from the northern slope of the Himalaya. *Earth and Planetary Science Letters*, *506*, 455–465. https://doi.org/10.1016/j.epsl.2018.11.002

Jahren, A. H., & Sternberg, L. S. L. (2002). Eocene meridional weather patterns reflected in the oxygen isotopes of Arctic fossil wood. *Geological Society of America Today*, *12*, 4–9. https://doi.org/10.1130/1052-5173(2002)012<0004:emwpri>2.0.co;2

Jahren, A. H., & Sternberg, L. S. L. (2003). Humidity estimate for the middle Eocene Arctic rain forest. *Geology*, *31*, 463–466. https://doi.org/10.1130/0091-7613(2003)031<0463:HEFTME>2.0.CO;2

Jahren, A. H., & Sternberg, L. S. L. (2008). Annual patterns within tree rings of the Arctic middle Eocene (ca. 45 Ma): Isotopic signatures of precipitation relative humidity, and deciduousness. *Geology*, *36*, 99–102. https://doi.org/10.1130/G23876A.1

Kahmen, A., Sachse, D., Arndt, S. K., Tu, K. P., Farrington, H., Vitousek, P. M., & Dawson, T. E. (2011). Cellulose δ18O is an index of leaf-to-air vapor pressure difference (VPD) in tropical plants. *Proceedings of the National Academy of Sciences*, *108*, 1981–1986. https://doi.org/10.1073/pnas.1018906108

Kassambara, A., & Mundt, F. (2020). *Factoextra: Extract and visualize the results of multivariate data analyses*. Retrieved From https://CRAN.R-project.org/package=factoextra

Kramer, P. J. (1943). Amount and duration of growth of various species of tree seedlings. *Plant Physiology*, *18*(2), 239.

Labotka, D. M., Grissino-Mayer, H. D., Mora, C. I., & Johnson, E. J. (2016). Patterns of moisture source and climate variability in the southeastern United States: A four-century seasonally resolved tree-ring oxygen-isotope record. *Climate Dynamics*, *46*, 2145–2154. https://doi.org/10.1007/s00382-015-2694-y

Leavitt, S. W., & Danzer, S. R. (1993). Method for batch processing small wood samples to holocellulose for stable-carbon isotope analysis. *Analytical Chemistry*, *65*, 87–89. https://doi.org/10.1021/ac00049a017

Lewis, D. B., Finkelstein, D. B., Grissino-Mayer, H. D., Mora, C. I., & Perfect, E. (2011). A multitree perspective of the tree ring tropical cyclone record from longleaf pine (Pinus palustris Mill.), Big Thicket National Preserve, Texas, United States. *Journal of Geophysical Research: Biogeosciences*, *116*. https://doi.org/10.1029/2009jg001194

Li, Z.-H., Labbé, N., Driese, S. G., & Grissino-Mayer, H. D. (2011). Micro-scale analysis of tree-ring δ18O and δ13C on α-cellulose spline reveals high-resolution intra-annual climate variability and tropical cyclone activity. *Chemical Geology*, *284*, 138–147. https://doi.org/10.1016/j.chemgeo.2011.02.015

Loader, N. J., Helle, G., Los, S. O., Lehmkuhl, F., & Schleser, G. H. (2010). Twentieth-century summer temperature variability in the southern Altai Mountains: A carbon and oxygen isotope study of tree-rings. *The Holocene*, *20*, 1149–1156. https://doi.org/10.1177/0959683610369507

Lukens, W. E., Nordt, L. C., Stinchcomb, G. E., Driese, S. G., & Tubbs, J. D. (2018). Reconstructing pH of paleosols using geochemical proxies. *Journal of Geology*, *126*, 427–449. https://doi.org/10.1086/697693

Managave, S. R., Sheshshayee, M. S., Ramesh, R., Borgaonkar, H. P., Shah, S. K., & Bhattacharyya, A. (2011). Response of cellulose oxygen isotope values of teak trees in differing monsoon environments to monsoon rainfall. *Dendrochronologia*, *29*, 89–97. https://doi.org/10.1016/j.dendro.2010.05.002

Managave, S. R., Shimla, P., Yadav, R. R., Ramesh, R., & Balakrishnan, S. (2020). Contrasting centennial-scale climate variability in high mountain asia revealed by a tree-ring oxygen isotope record from Lahaul-Spiti. *Geophysical Research Letters*, *47*, e2019GL086170. https://doi.org/10.1029/2019GL086170

Mandal, U. K., Warrington, D. N., Bhardwaj, A. K., Bar-Tal, A., Kautsky, L., Minz, D., & Levy, G. J. (2008). Evaluating impact of irrigation water quality on a calcareous clay soil using principal component analysis. *Geoderma*, *144*, 189–197. https://doi.org/10.1016/j.geoderma.2007.11.014

Menne, M. J., Williams, C. N., Gleason, B. E., Rennie, J. J., & Lawrimore, J. H. (2018). The global historical climatology network monthly temperature dataset, version 4. *Journal of Climate*, *31*(24), 9835–9854. https://doi.org/10.1175/JCLI-D-18-0094.1

Miller, D. L., Mora, C. I., Grissino-Mayer, H. D., Mock, C. J., Uhle, M. E., & Sharp, Z. (2006). Tree-ring isotope records of tropical cyclone activity. *Proceedings of the National Academy of Sciences*, *103*, 14294–14297. https://doi.org/10.1073/pnas.0606549103

Mora, C. I., Miller, D. L., & Grissino-Mayer, H. D. (2007). Oxygen isotope proxies in tree-ring cellulose: Tropical cyclones, drought, and climate oscillations. *Terrestrial Ecology*, *1*, 63–75. https://doi.org/10.1016/s1936-7961(07)01005-6

Moustakis, Y., Papalexiou, S. M., Onof, C. J., & Paschalis, A. (2021). Seasonality, intensity, and duration of rainfall extremes change in a warmer climate. *Earth's Future*, *9*. https://doi.org/10.1029/2020ef001824

Palmer, W. C. (1965). *Meteorological drought* (p. 30). US Department of CommerceWeather Bureau.

Qin, C., Yang, B., Bräuning, A., Grießinger, J., & Wernicke, J. (2015). Drought signals in tree-ring stable oxygen isotope series of Qilian juniper from the arid northeastern Tibetan Plateau. *Global and Planetary Change*, *125*, 48–59. https://doi.org/10.1016/j.gloplacha.2014.12.002

R Core Team. (2020). *RStudio v 3.6.1*.

Richter, S. L., Johnson, A. H., Dranoff, M. M., LePage, B. A., & Williams, C. J. (2008). Oxygen isotope ratios in fossil wood cellulose: Isotopic composition of Eocene- to Holocene-aged cellulose. *Geochimica et Cosmochimica Acta*, *72*, 2744–2753. https://doi.org/10.1016/j.gca.2008.01.031

Richter, S. L., Johnson, A. H., Dranoff, M. M., & Taylor, K. D. (2008). Continental-scale patterns in modern wood cellulose δ18O: Implications for interpreting paleo-wood cellulose δ18O. *Geochimica et Cosmochimica Acta*, *72*, 2735–2743. https://doi.org/10.1016/j.gca.2008.01.030

Robinson, D., Hayes, A., & Couch, S. (2021). *Broom: Convert statistical objects into tidy tibbles*. Retrieved From https://CRAN.R-project.org/package=broom

Roden, J. S., Lin, G., & Ehleringer, J. R. (2000). A mechanistic model for interpretation of hydrogen and oxygen isotope ratios in tree-ring cellulose. *Geochimica et Cosmochimica Acta*, *64*, 21–35. https://doi.org/10.1016/s0016-7037(99)00195-7

Roque-Malo, S., & Kumar, P. (2017). Patterns of change in high frequency precipitation variability over North America. *Scientific Reports*, *7*, 10853. https://doi.org/10.1038/s41598-017-10827-8

Roy, A. J., & Midkiff, C. T. (1988). *Soil survey of Calcasieu parish* (p. 86). United States Department of Agriculture.

Sano, M., Sheshshayee, M. S., Managave, S. R., Ramesh, R., Sukumar, R., & Sweda, T. (2010). Climatic potential of δ18O of Abies spectabilis from the Nepal Himalaya. *Dendrochronologia*, *28*, 93–98. https://doi.org/10.1016/j.dendro.2009.05.005

Schollaen, K., Heinrich, I., Neuwirth, B., Krusic, P. J., D'Arrigo, R. D., Karyanto, O., & Helle, G. (2013). Multiple tree-ring chronologies (ring width, δ13C and δ18O) reveal dry and rainy season signals of rainfall in Indonesia. *Quaternary Science Reviews*, *73*, 170–181. https://doi.org/10.1016/j.quascirev.2013.05.018

Schubert, B. A., & Jahren, A. H. (2015). Seasonal temperature and precipitation recorded in the intra-annual oxygen isotope pattern of meteoric water and tree-ring cellulose. *Quaternary Science Reviews*, *125*, 1–14. https://doi.org/10.1016/j.quascirev.2015.07.024

Shi, F., Rao, Z., Li, Y., Cao, J., Shi, X., Li, C., & Sun, W. (2019). Precipitation δ18O recorded by the α-cellulose δ18O of plant residues in surface soils: Evidence from a broad environmental gradient in inland China. *Global Biogeochemical Cycles*, *33*, 1440–1468. https://doi.org/10.1029/2019gb006418

Shi, S., Shi, J., Xu, C., Leavitt, S. W., Wright, W. E., Cai, Z., et al. (2020). Tree-ring δ18O from Southeast China reveals monsoon precipitation and ENSO variability. *Palaeogeography, Palaeoclimatology, Palaeoecology*, *558*, 109954. https://doi.org/10.1016/j.palaeo.2020.109954

Sternberg, L. D. S. L. O. (2009). Oxygen stable isotope ratios of tree-ring cellulose: The next phase of understanding. *New Phytologist*, *181*, 553–562. https://doi.org/10.1111/j.1469-8137.2008.02661.x

Treydte, K., Frank, D., Esper, J., Andreu, L., Bednarz, Z., Berninger, F., et al. (2007). Signal strength and climate calibration of a European tree-ring isotope network. *Geophysical Research Letters*, *34*. https://doi.org/10.1029/2007GL031106

Vachon, R.W., White, J.W., Gutmann, E., & Welker, J.M. (2007). Amount-weighted annual isotopic (δ18O) values are affected by the seasonality of precipitation: A sensitivity study. *Geophysical Research Letters*, *34*. https://doi.org/10.1029/2007GL030547

Verheyden, A., Helle, G., Schleser, G. H., Dehairs, F., Beeckman, H., & Koedam, N. (2004). Annual cyclicity in high-resolution stable carbon and oxygen isotope ratios in the wood of the mangrove tree Rhizophora mucronata. *Plant Cell & Environment*. *27*. 1525–1536. https://doi.org/10.1111/j.1365-3040.2004.01258.x

Wickham, H., Averick, M., Bryan, J., Chang, W., McGowan, L. D., François, R., et al. (2019). Welcome to the Tidyverse. *Journal of Open Source Software*, *4*, 1686. https://doi.org/10.21105/joss.01686

Xu, C., Pumijumnong, N., Nakatsuka, T., Sano, M., & Li, Z. (2015). A tree-ring cellulose δ18O-based July–October precipitation reconstruction since AD 1828, northwest Thailand. *Journal of Hydrology*, *529*, 433–441. https://doi.org/10.1016/j.jhydrol.2015.02.037

Xu, C., Sano, M., Dimri, A. P., Ramesh, R., Nakatsuka, T., Shi, F., & Guo, Z. (2018). Decreasing Indian summer monsoon on the northern Indian sub-continent during the last 180 years: Evidence from five tree-ring cellulose oxygen isotope chronologies. *Climate of the Past*, *14*, 653–664. https://doi.org/10.5194/cp-14-653-2018

Xu, C., Zheng, H., Nakatsuka, T., Sano, M., Li, Z., & Ge, J. (2016). Inter-and intra-annual tree-ring cellulose oxygen isotope variability in response to precipitation in Southeast China. *Trees*, *30*, 785–794. https://doi.org/10.1007/s00468-015-1320-2

Yang, B., Qin, C., Bräuning, A., Osborn, T. J., Trouet, V., Ljungqvist, F. C., et al. (2021). Long-term decrease in Asian monsoon rainfall and abrupt climate change events over the past 6,700 years. *Proceedings of the National Academy of Sciences*, *118*, e2102007118. https://doi.org/10.1073/pnas.2102007118